BNL-203292-2018-TECH

CBETA/021

Beam dynamics validation of the Halbach Technology FFAG Cell for Cornell-BNL Energy Recovery Linac

F. Méot

January 2018

Collider Accelerator Department

Brookhaven National Laboratory

U.S. Department of Energy

USDOE Office of Science (SC), Nuclear Physics (NP) (SC-26)

DISCLAIMER

Beam dynamics validation of the Halbach Technology FFAG Cell for Cornell-BNL Energy Recovery Linac

F. Méot, N. Tsoupas, S. Brooks, D. Trbojevic

Collider-Accelerator Department, BNL, Upton, NY 11973

January 29, 2018

Abstract

The Cornell-BNL Electron Test Accelerator (CBETA), a 150 MeV energy recovery linac (ERL) now in construction at Cornell, employs a fixed-field alternating gradient (FFAG) optics return loop: a single beam line comprised of quadrupole doublet cells, which accepts four recirculated energies. CBETA FFAG cell uses Halbach permanent magnet technology, its design studies have covered an extended period of time supported all the way by extensive particle dynamics simulations using computed 3-D field map models. This approach, which supported the choice of Halbach technology for CBETA FFAG ERL in 2016, is discussed and illustrated here based on the final stage in these beam dynamics studies, namely the validation of a ultimate, optimized design of the cell.

Note CBETA/021
BNL C-AD

Contents

1 Introduction

The Cornell Laboratory of Accelerator-based Sciences and Education (CLASSE) and the Collider Accelerator Department (BNL-CAD) are developing a multi-turn energy recovery linac (ERL) [1, 2] (Fig. 1) based on Cornell's 80 MeV, 1.3 GHz RF, superconducting linac and on a Non-Scaling Fixed Field Alternating Gradient (NS-FFAG) return loop [3] using Halbach permanent magnet quadrupole technology [4].

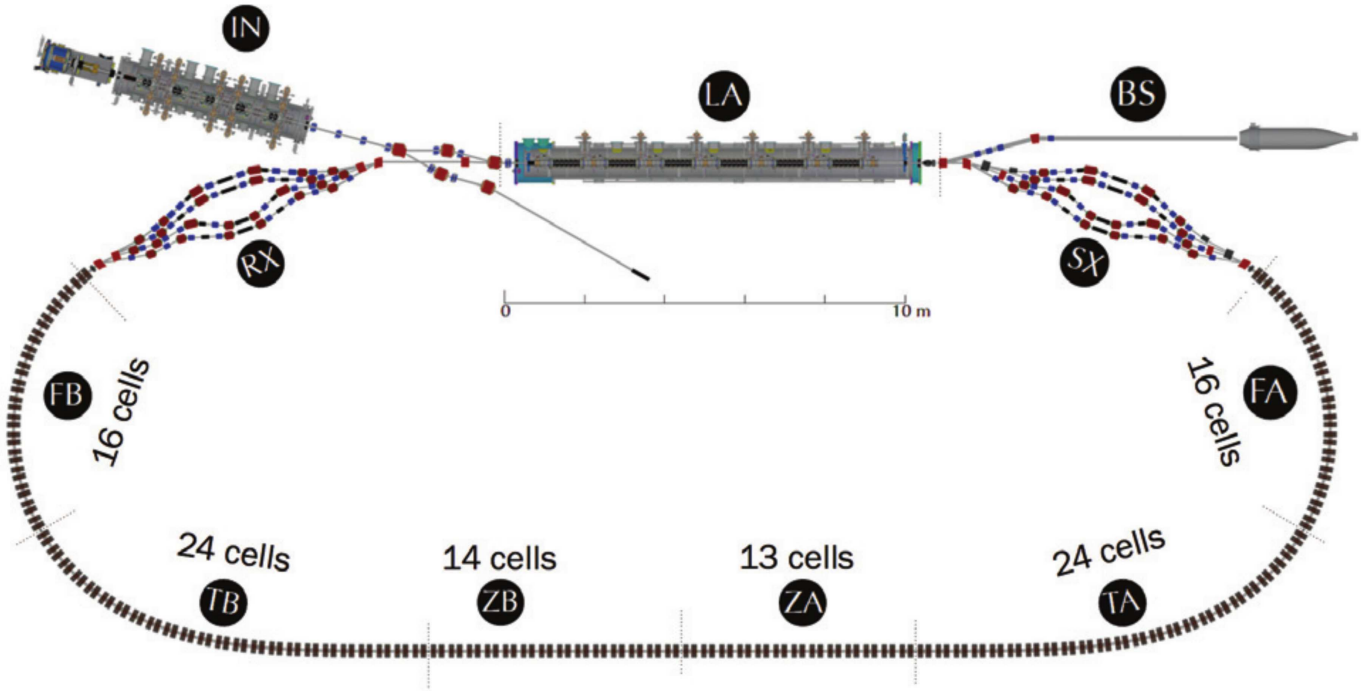

Figure 1: [1] CBETA 150 MeV, 4-pass, 79 m circumference ERL, based on a 36 MeV superconducting linac and a 107 cell NS-FFAG return loop using Halbach permanent magnet quadrupole technology.

The 6 MeV electron bunches from the injector ("IN" section in Fig. 1) are accelerated in four passes through the linac operated at 36 MeV ("LA"), to successively 42, 78, 114 and 150 MeV. After reaching 150 MeV the bunches are brought back to the linac with a prior $\lambda/2$ phase shift with respect to the linac RF wave, for deceleration. Energy is recovered down to the 6 MeV injection value after an additional 4-pass through the linac, and bunches are then sent to a beam stop ("BS").

The ERL recirculation proper presents several specificities:

- a single return loop based on NS-FFAG optics [3] ("FA" through "FB" sections in Fig. 1) accepts the four different energies on their way up to 150 MeV and back down to 6 MeV. The loop takes the bunches from a spreader line located at the downstream end of the linac ("SX"), and guides them back to a combiner line located at the upstream end of the linac ("RX"), via two arcs ("FA", "FB"), two dispersion suppression sections ("TA" and "TB"), and a long straight section ("ZA-ZB");

- the FFAG loop magnets are based on Halbach permanent magnet technology, including dipole and quadrupole window frame windings mounted around the magnets, and including tight high-order multipole correction using a technique of in-bore short wires [4, 5];

- in the arcs the cell is a quadrupole and combined function dipole doublet (Figs. 2, 3), with the latter an asymmetric cross-section version of the former [2]; in the long straight both cell magnets are pure quadrupoles and they are aligned;

- the dispersion suppression sections merge the separated 42, 78, 114 and 150 MeV orbits, from the arcs where they radially span up to 4.66 cm (in QF), onto a common axis in the long straight section [2]; in these sections the FFAG cell slowly evolves from a 5 degree bend at its arc end, to no-bend at its long straight end.

The present article focuses on the 3-D OPERA [6] field map based beam dynamics studies performed to qualify the Halbach CBETA FFAG cell, a period of time of a few years which saw the design of numerous intermediate 3-D field map computation and beam dynamics simulations. The details of the optics methods, criteria, theoretical approach to the cell parameters, as well as the numerous methodical Halbach magnet prototyping studies which yielded the present CBETA arc cell, can be found in the many dedicated publications [5, 7, 8, 9, 10, 11, 12].

To summarize briefly that phase of the studies: the first designs of the Halbach technology FFAG cell for CBETA inherited from the linac-ring eRHIC EIC studies [7]. They accounted for a 67-250 MeV 4-pass recirculation using Cornell linac at 61 MeV, and included magnet prototyping which eventually led to a proof-of-principle 8-cell Halbach FFAG arc, successfully operated at BNL Accelerator Test Facility in 2017 [12]. The ERL energy was later scaled down to 150 MeV in order to account for a possible use of, instead, an iron dominated permanent magnet design which was being studied in parallel [13]. This in consequence led to a 150 MeV version on the Halbach cell side [5], which ended up as the technology retained for the ERL return loop, at the end of 2016.

The latest stages of the beam dynamics studies performed in support to the Halbach design are addressed here. Section 2 introduces to the field maps used in the simulations, Sec. 3 describes the resulting paraxial parameters of the cell and set the landscape for the large amplitude and resonance studies addressed in Sec. 4. Section 5 concludes with the dynamical admittance of a 300-cell channel.

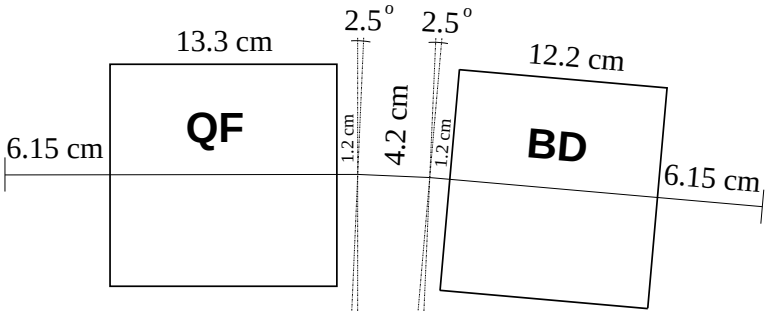

Figure 2: A synoptic of CBETA 5-degree bend, 44.4 cm long arc cell. QF is a pure quadrupole, focusing, BD is a combined function dipole, defocusing. The optical axis coincides with the bore axis in the Halbach magnets.

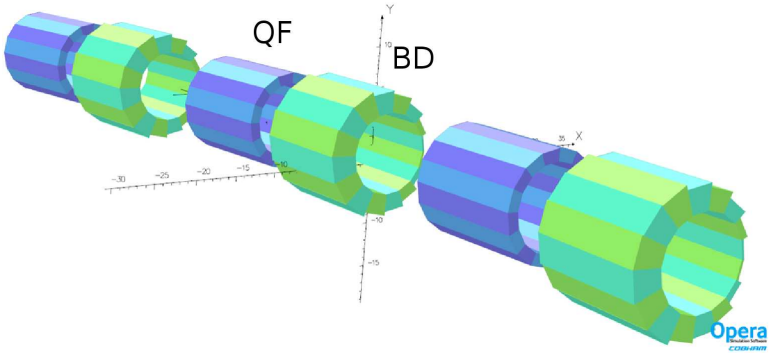

Figure 3: The 3-cell model in OPERA. The field map of the central (QF,BD) doublet is used in the case of the full-cell, single-map ray-tracing simulations.

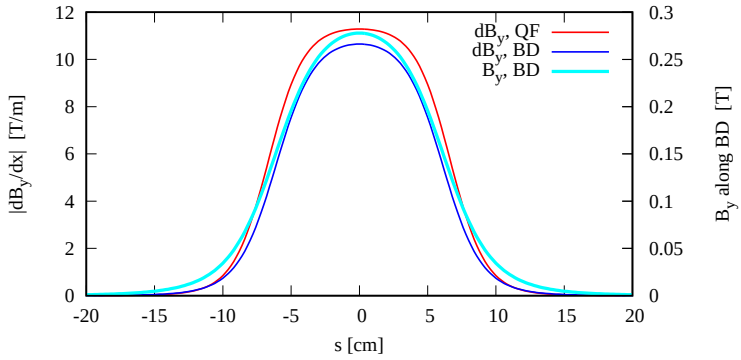

Figure 4: Quadrupole gradients $\mathrm{dB_y(s)/dx}$ (the two thin curves) along the bore axes of QF (higher field curve, red) and BD (lower field curve, blue), and vertical dipole field component $\mathrm{B_y}$ (intermediate, thicker curve) along BD axis.

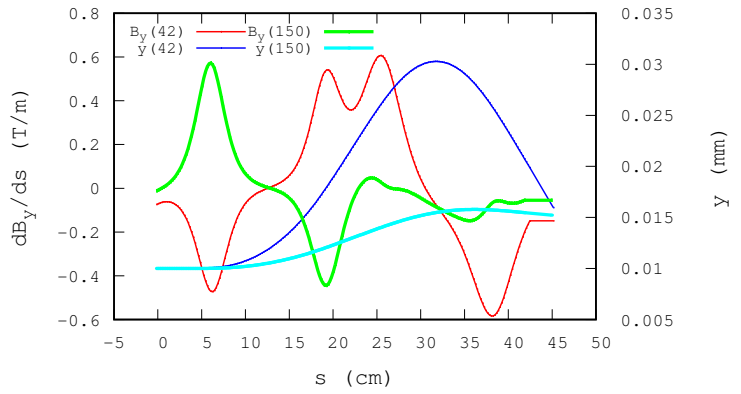

Figure 5: Vertical coordinate (right vertical axis) and first order derivatives dB_y/ds (left vertical axis) along a 42 MeV (thick curves) and a 150 MeV (thiner curves) off-mid plane trajectory across the cell.

2 Three-dimensional field maps of the QF and BD magnets

Accurate properties of FFAG cells can only be determined based on accurate field models, that holds for orbits, focusing and higher order parameters including chromaticity, amplitude detuning, dynamical admittance and other feed down [14, 15, 16, 17, 18]. In the CBETA FFAG cell magnets are short with a large aperture to length ratio, they are close to each other (Fig. 2), field fall-offs overlap, fields have some non-linear content, periodic stability limits as well as nearby resonances are a concern, large amplitude motion has to be explored to hunt possible limitations. For these reasons field maps from an OPERA 3-D model of the cell (Fig. 3) are used. On the other hand using field maps requires stepwise integration of the equations of motion and this contributes to the accuracy of the computer modeling of the dynamics. A reference in that matter: the field map approach revealed useful in the EMMA NS-FFAG ring accelerator experiment[1] [19] and contributed fruitful learnings [20].

Table 1: Parameters of the cell quadrupoles, as of the 3-D OPERA field maps used in the simulations. The dipole field integral $\int \mathrm{B(z)dz}$ and gradient integral $\int \frac{\mathrm{dB}}{\mathrm{dx}}\mathrm{(z)dz}$ are taken along the bore axis. In optimizing the cell parameters, these field and gradient values are applied a normalization factor ("norm.", col. 5), whereas BD is still allowed a (presumably small) radial shift with respect to QF ("shift", col. 6), this is discussed in the foregoing.

	length $\mathcal{L}$ (cm)	$\int \mathrm{B(z)dz}$ (T m)	$\frac{1}{\mathcal{L}}\int \frac{\mathrm{dB}}{\mathrm{dx}}\mathrm{(z)dz}$ (T/m)	norm.	shift (μm)
QF	13.3	0	11.8451	0.96987	-
BD	12.2	0.3155	11.4207	0.96987	3.6

Due to the large bore to length ratio of the magnets the field and transverse gradient along the orbits do not feature any plateau (Fig. 4) which contributes a non-linear content (Fig. 5) as expected from the multipole scalar potential from which the field derives,

$$V_1(s,x,y) = G_1(s)y - \frac{G_1^{(2)}(s)}{8}(x^2+y^2)y + \frac{G_1^{(4)}(s)}{192}(x^2+y^2)^2y + ... \quad \text{(dipole)}$$

$$V_2(s,x,y) = G_2(s)xy - \frac{G_2^{(2)}(s)}{12}(x^2+y^2)xy + \frac{G_2^{(4)}(s)}{384}(x^2+y^2)^2xy + ... \quad \text{(quadrupole)}$$

with s, x, y respectively the longitudinal, radial and vertical coordinates in the magnets, $G_{1,2}(s)$ the longitudinal form factor and $G_{1,2}^{(n)} = d^nG_{1,2}/ds^n$. Note that non-zero vertical motion introduces non-linear coupling.

Dedicated OPERA studies address error and correction aspects based on external coils for linear corrections and high-order multipole compensation by a method of in-bore wires [4, 5], this is out of the scope here, magnet geometry is assumed perfect, the only sources of non-linearities are, (i) the multipole content intrinsic to the magnet geometry in the OPERA simulation and (ii) the longitudinal form factor $\mathrm{G(s)}$. These intrinsic multipoles are addressed indirectly here: their effects appear weak enough that the admittance of this essentially linear FFAG cell, as long as tunes are kept distant from a couple of well determined resonances, remains very large (section 4).

A synoptic of the arc cell is given in Fig. 2. "QF" is a pure focusing quadrupole, the lopsided shape of "BD" (Fig. 3) makes it a combined function dipole, defocusing here [12]. Gradients along QF and BD axes and dipole field component along BD axis, from their individual field maps, are shown in Fig. 4. The origin of the OPERA frame is at the center of the bore. Geometry and field values are summarized in Tab. 1.

Tracking simulations in support to the cell design have used two series of 3-D field maps:
- as a first approach in the design and optimization period, pairs of independent field maps, each quadrupole its own,
- in a later stage, closer to the finalization of the cell parameters, one single map encompassing the complete quadrupole doublet and its fringe fall-offs.

The OPERA model in the second case is displayed in Fig. 3. A three-cell section is simulated and the field map of the central cell is used for the ray-tracing simulations, on the hypothesis that it yields a better representation of the periodicity of the field. This has been verified to hold to sufficient accuracy, by checking the continuity of the periodic field and derivatives at both ends in the useful field region.

3 Paraxial optical properties

The goal here is essentially to establish the transverse paraxial cell properties, as a premise to the large amplitude transverse motion, next section.

The relative positioning of successive cells in the CBETA return loop is fixed at this latest stage of cell parameter optimization. However a latest iteration on their respective field values and of their relative positioning is still possible, it requires using the individual field maps of QF and BD. The constraints in this final adjustment are
(i) the requested 5 degree deviation of the periodic orbits,
(ii) balanced extreme orbit excursion in QF.
The two variables available are
(i) a normalization factor on the OPERA field, which will end up about 0.97 (col. 5 in Tab. 1), to be taken care for the bulk of it during the permanent magnet assembling [12],
(ii) the relative positioning of BD in the cell, which ends up to be a marginal few micrometers.

Following this optimization, a single OPERA map of the complete cell has been produced, this will be addressed further in the foregoing.

[1] The EMMA FFAG (Electron Model for Many Application) experiment took place at Daresbury in the 2005-2012 period. It studied a prototype 10 to 20 MeV NS-FFAG ring accelerator. The EMMA cell was based on a similar optics: a pair of electromagnetic quadrupoles, radially shifted with respect to one another to create a net bending.

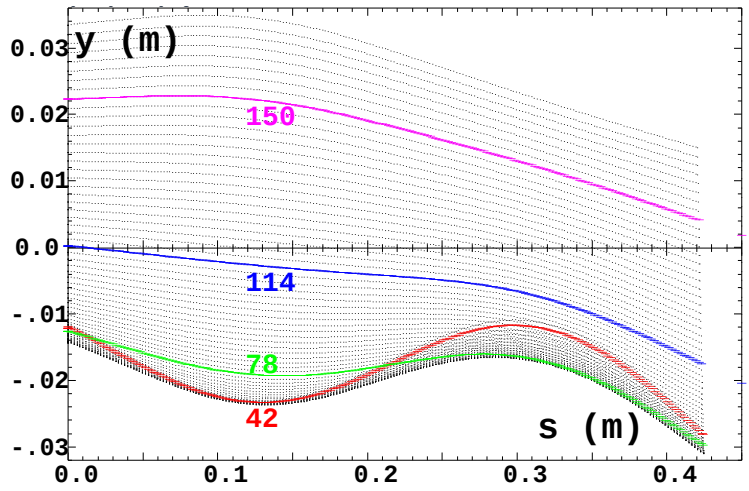

Figure 6: A scan in energy of periodic orbits across the 3-D full-cell map, 64 different energies over a 40-166 MeV range, the 4 design energies are thicker, colored curves. The 42 and 150 MeV orbit excursions reach ∓ 2.33 cm respectively, *wrt* QF bore axis. Nominal beam envelopes extend a fraction of a millimeter about these orbits.

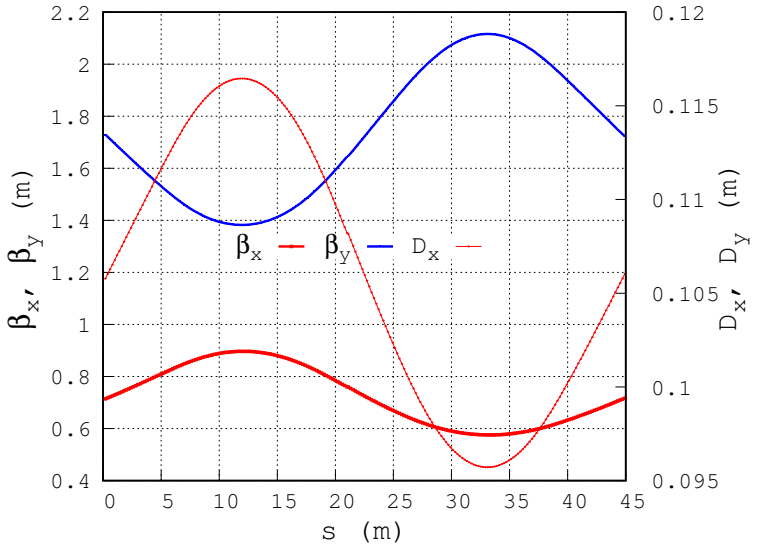

Figure 7: Optical functions along the cell, 150 MeV case.

Resulting orbits at various energies across the cell are shown in Figs. 6, The betatron functions do not exceed 2.1 meters (Fig. 7 and Tab. 2); given bunch emittances $\epsilon_{x,y} = 1\,\pi\mu$m, *rms*, normalized, it means that beam envelopes extend a fraction of a millimeter about the orbits. B_y field component along the latter is shown in Fig. 8.

Figure 9 shows a scan in energy of paraxial tunes and natural chromaticities. The periodic stability limit at low energy is due to the cell-tune approaching a half-integer value. At high energy it stems from the evolution of the wedge angle. The third integer $\mathrm{Q_x} = 1/3$ resonance is avoided, the resonance $\mathrm{Q_x} + 2\mathrm{Q_y} = 1$ as well, this is addressed further in Sec. 4. These considerations are part of the cell parameters optimization: the high energy stability limit had to be pushed away enough from the maximum design energy, 150 MeV; the 42 and 78 MeV energies had to be placed distant enough from $\mathrm{Q_x} + 2\mathrm{Q_y}$ =integer.

Outcomes of both approaches, *i.e.*, separate QF and BD field maps and a single full-cell field map, are superimposed in these figures. The agreement between the two series of results validates the two methods. a useful flexibility which can be exploited in further start-to-end 6-D bunch transport simulations in the complete ERL, an on-going work. Details of the paraxial parameters of the 4 design energies are given in Tab. 2.

Finally, given the very small dispersion function of the NS-FFAG cell, a maximum amplitude in the few centimeters (Tab. 2), CBETA beam momentum spread, with a nominal value below 10^{-3} *rms*, has marginal effect on beam envelopes.

4 Large amplitude motion

Large amplitude transverse motion is inspected in this section. The maximum 300-cell stable amplitudes, at the four design momenta, are displayed in Figs. 10, 11 for the horizontal and vertical motions respectively. The 114 MeV energy which features the largest stable amplitudes,

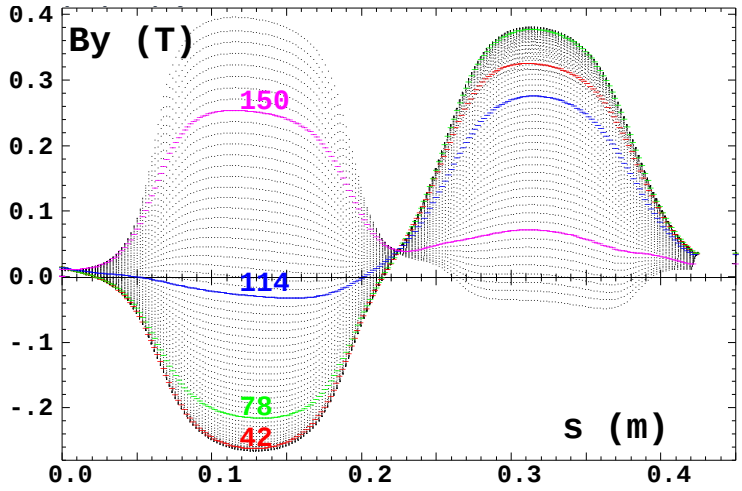

Figure 8: Vertical field component along 64 different orbits (40 to 166 MeV) across the cell, including the 4 design energies (thick colored lines).

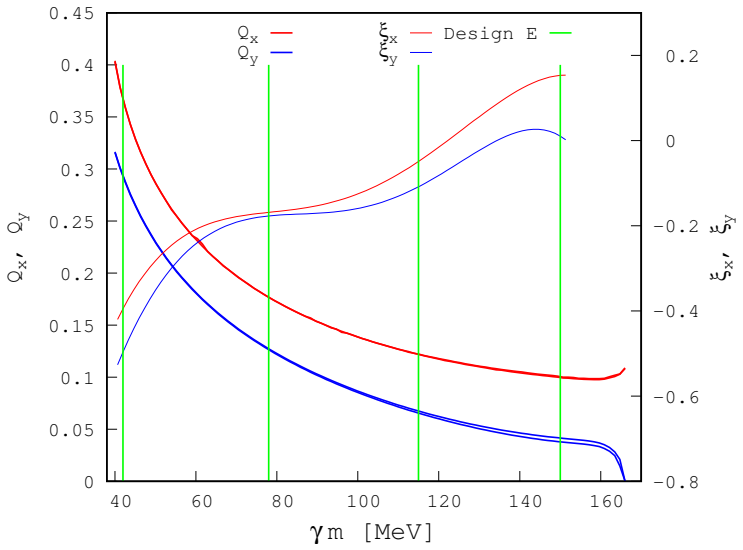

Figure 9: Energy dependence of cell tunes and chromaticities, from 40 MeV to the maximum stable energy, 166 MeV. Tunes from both separate quadrupole maps, or single full-cell map, are superimposed for comparison of the two approaches. Vertical bars are at design energies.

horizontal and vertical, appears to be in the region of maximum dynamical admittance (Fig. 12); its being centered closest to QF and BD axes (Fig. 6) where field non-linearities have weaker effect could be the reason for that. The corresponding invariant and tune values are detailed in Tab. 3. A scan of the maximum 300-cell stable invariant value, over the energy interval 40-166 MeV, is displayed in Fig. 12, it is only weakly dependent on the number of cells beyond about 200 cells. The observed dip at E=44.8 MeV in the case of the horizontal invariant is at $Q_x = 1/3$. The sharp fall at 40.87 MeV in the case of the vertical invariant is in the vicinity of the resonance line $Q_x + 2Q_y = 1$ ($Q_x = 0.388707$, $Q_y = 0.305353$).

One may question the validity of the field extrapolation from the OPERA field map by the numerical stepwise method [21], given the limited vertical extent of the maps used in these tracking simulations, namely $\Delta y = \pm 1.3$ cm. The computation appears to behave reasonably: in QF the trajectories at maximum horizontal and vertical amplitudes are within the 3-D limits of the field map (which extends over ± 4.1 cm $\times \pm 1.3$ cm $\times \pm 25$ cm in H$\times$V$\times$Longitudinal). Regarding the trajectories in the combined function dipole BD, their vertical excursion goes far beyond vertical field map limits (± 2.6 cm, Fig. 13), however the field extrapolated from the map shows a consistent evolution in value and shape with y excursion. This is considered a significant enough approach of the actually very large admittance, with stable trajectories comprised at least within the field map extent.

Fig. 14 shows the motion footprint in tune diagram, for a small set of particles with invariants evenly spread from paraxial to the maximum stable amplitude (namely, horizontal tunes correspond to Fig. 10 invariants, vertical ones correspond to Fig. 11). The optimization of the cell has accounted for maintaining the paraxial working point distant enough from the potentially harmful coupling lines [5], "$Q_x = 2Q_y$" in the 114 and 150 MeV regions, "$Q_x + 2Q_y = 1$" and "$2Q_x + Q_y = 1$" in the 42 MeV region. The first two resonances can be excited by upright sextupole components (present for all energies as all orbits are off-axis in the quadrupoles), the third one requires a skew sextupole non-linearity. These considerations are relevant to multipole tolerances, which is out of the scope here. Note also, the $Q_x = 2Q_y$ resonance line is akin to the Walkinshaw resonance ($Q_x \approx \gamma > 1$ in cyclotrons), a mechanism for emittance growth by emittance exchange, in cyclotrons. Fig. 15 shows that these amplitude detuning effects are far beyond nominal CBETA bunch emittance and other defect and emittance growth margins [1].

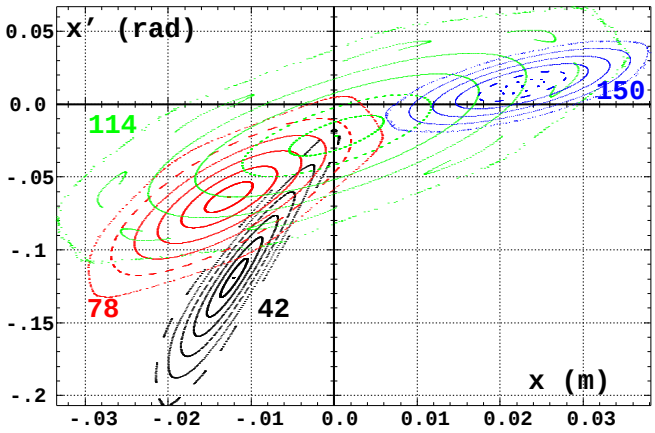

Figure 10: For each of the 4 design energies, seven particles are tracked over 300 cells, all pure horizontal motion, with increasing invariant values from small to maximum stable amplitude.

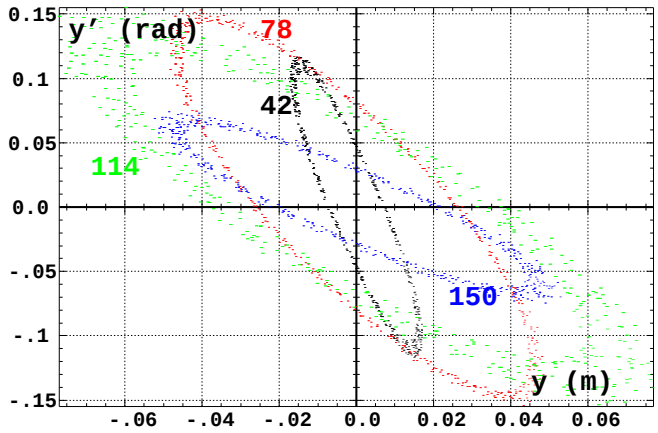

Figure 11: Vertical invariants at maximum stable amplitude at the 4 design energies, for a 300-cell tracking.

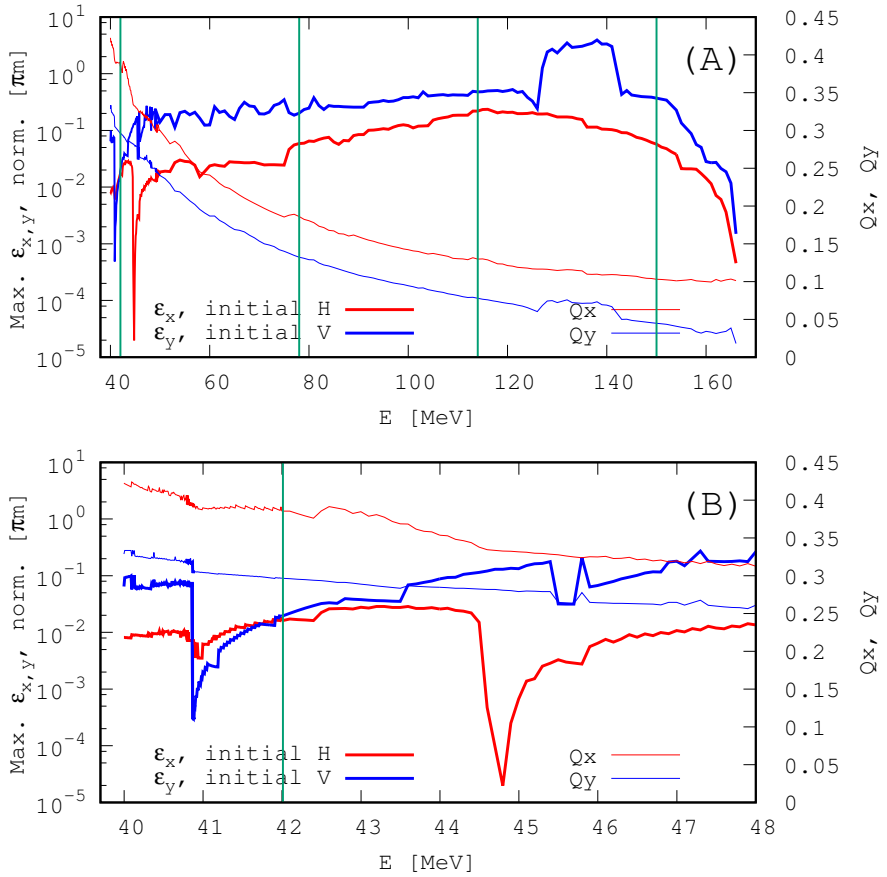

Figure 12: A scan of the horizontal (red) and vertical (blue) dynamical admittances of a 300-cell FFAG arc, (A) over 40-166 MeV and (B) a zoom in the region 40-48 MeV (the quantity plotted here is the surface of the phase space invariant at maximum stable amplitude, respectively horizontal as shown in Fig. 10, and vertical in Fig. 11). Vertical bars are at the design energies 42, 78, 114 and 150 MeV. The dip in the horizontal admittance in the 45 MeV region is at $Q_x = \frac{1}{3}$. The dip in the vertical admittance in the 41 MeV region is at $Q_x + 2Q_y = 1$. Q_x and Q_y tune values plotted are at maximum stable amplitude.

Table 2: In the CBETA arc cell, for the four design energies: peak values of the orbit excursion, dispersion, betatron functions (cols. 2-5), orbit length (col. 6), and paraxial tunes (cols. 7, 8),

γmc^2 (MeV)	$\hat{x}$ (cm)	$\hat{D}_x$ (m)	$\hat{\beta}_x$ (m)	$\hat{\beta}_y$ (m)	s (cm)	Q_x	Q_y
150	2.33	0.117	0.9	2.1	44.58	0.0999	0.0418
114	0.58	0.069	0.78	1.38	44.39	0.1227	0.0685
78	1.85	0.024	0.65	0.88	44.33	0.1768	0.1272
42	2.33	0.017	0.93	0.8	44.49	0.3672	0.294

Table 3: Maximum 300-cell stable invariant values, normalized, for the four design energies. Col. 2: case of horizontal motion with zero vertical invariant. Col. 3: case of vertical motion with quasi-zero horizontal invariant. Tunes in cols. 4, 5 correspond to maximum amplitude motions in respectively cols. 1 and 2; they are given for comparison with the paraxial values in Tab. 2.

γmc^2 (MeV)	max. ϵ_x (πmm)	max. ϵ_y (πmm)	Q_x	Q_y
150	16.4	111	0.10298	0.04640
114	82.5	176	0.12968	0.07788
78	32.2	108	0.18632	0.13251
42	16.4	19.3	0.38551	0.29670

5 Transmission of a 300-cell beam line

The previous results demonstrate the largely linear properties of the CBETA cell, as long as the working energy is maintained away from potentially harmful resonances. In these conditions, the earlier 300-cell admittance results point to a large transmission.

These properties are confirmed here, by an estimate of the "dynamical admittance" as seen from the entrance of the 300-cell beam-line. By "dynamical admittance" it is meant that (i) no geometrical transverse obstacle is introduced in the line, (ii) particles are lost because they experience strong fields arising due to large transverse excursion.

Considering 300 cells, which is about 3 times the total number of cells in the CBETA return FFAG loop, is an arbitrary choice, a large value in view essentially of a safe margin in this estimate. A reason to allow margin is that these bunch transmission simulations consider a defect-free return loop, exempt of any emittance growth effects other than (i) field non-linearities intrinsic to the OPERA model as discussed earlier, and (ii) kinematic non-linearities which are present to high order due to the stepwise ray-tracing method [21].

The transmission simulation operates in the following manner: a 4-D (zero longitudinal emittance), 10,000 particle bunch is launched through the beam line; it has initial Gaussian transverse emittances taken far beyond transverse admittance, for instance in the 42 MeV case, *rms* $\epsilon_{x,y} = 20\,\pi$mm. All particles with invariants beyond admittance will be lost at some azimuth during the transport, thus the admittance is taken to be the emittance of the survived 4-D bunch at the end of the line.

Figures 16, 17 show the transmitted distributions together with the initial distribution of the particles which make it to the end, in the 42 MeV case as an illustration: of the initial 10,000 particles, about 25% survive and determine the horizontal and vertical admittances of the channel, seen from its entrance, for that energy, namely $\epsilon_x = 4\,\pi$mm, $\epsilon_y/\pi = 15\,\pi$mm, normalized. Closer inspection shows that particles that survive the transport have essentially unchanged elliptical invariants, thus the motion within the admittance window is linear (and 300 cells is too small a number for weak resonances to possibly develop). The exercise was repeated for 78, 114 and 150 MeV, results are gathered in Tab. 4, they can be compared to the maximum stable invariant values in Fig. 12: quantities in both series of data appear commensurate, as expected.

In conclusion the admittance of the line is, in both planes and for all four design energies, more than 3 orders of magnitude beyond the bunch nominal emittances $\epsilon_{x,y} = 1\,\pi\mu$m, normalized.

Momentum spread has negligible effect, on closed orbits and beam envelopes due to the small dispersion ($\hat{\mathrm{D}}_\mathrm{x} < 12$ cm, Tab. 2), and on periodic betatron functions due to the small chromaticity (Fig. 9). Transmission simulations show that an extreme $\sigma_{\delta \mathrm{p/p}} = 10^{-3}$ leaves the results in Tab. 4 essentially unchanged.

Table 4: Normalized horizontal (col. 2) and vertical (col. 3) dynamical admittance of a 300-cell beam line. This is the transverse emittances of the 4-D bunch of mono-energetic particles that have survived the transport through the line. Momentum spread in the bunch has marginal effect on these data.

γmc^2 (MeV)	A_x (πmm)	$\mathrm{A_y}$ (πmm)
150	19	37
114	70	154
78	22	52
42	7	13

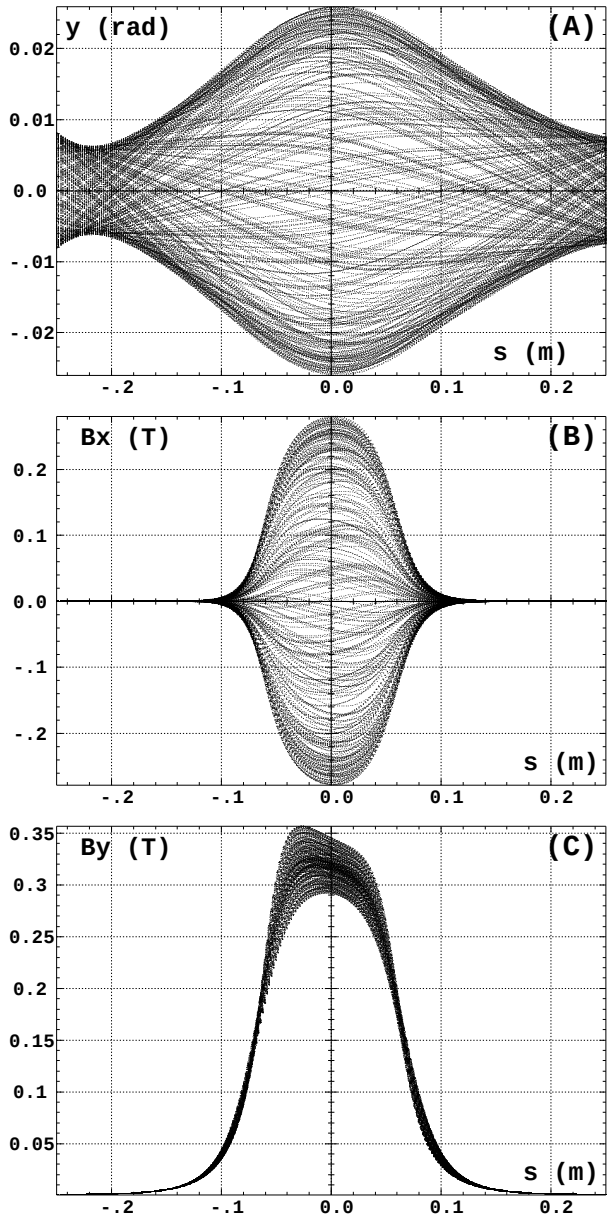

Figure 13: (A) y projection of the 42 MeV periodic motion at maximum vertical stable amplitude, across BD, over a few tens of passes. (B) and (C), respectively : corresponding radial and vertical components of the field experienced over these passes across BD.

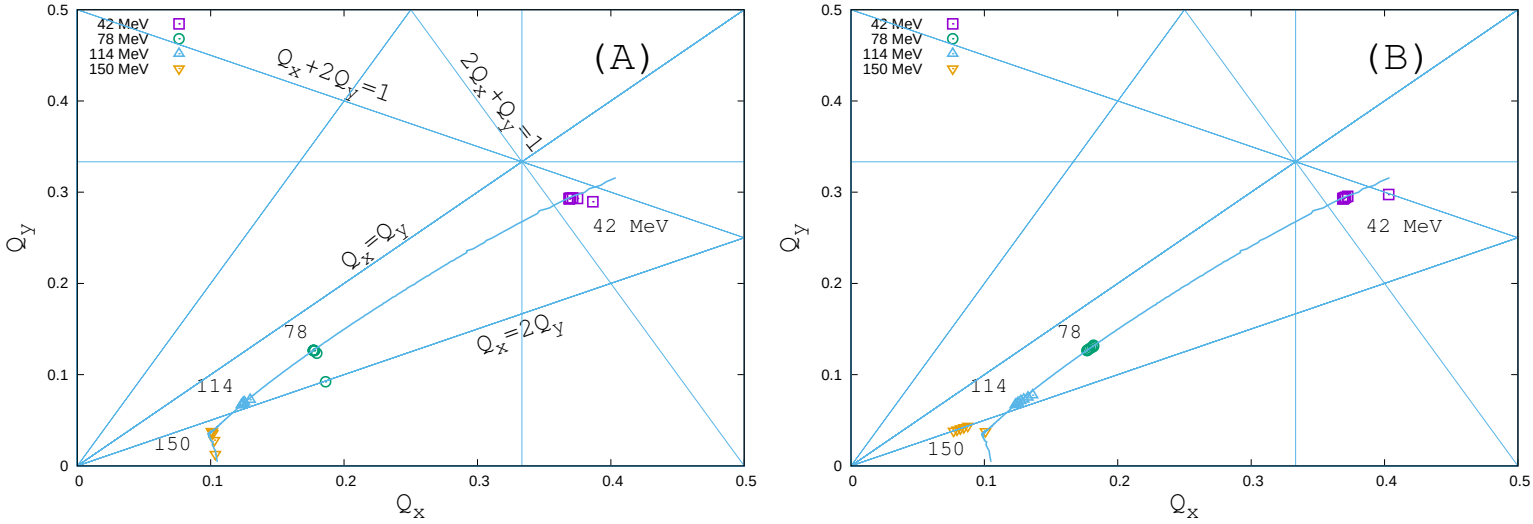

Figure 14: The solid curve (the same in both (A) and (B)) represents the paraxial tune path in the periodic stability interval 40-166 MeV. Markers represent the tune values at large transverse motion amplitude, for a series of invariant values up to the largest. (A) case of horizontal motion with paraxial vertical invariant; (B) case of vertical motion with paraxial horizontal invariant.

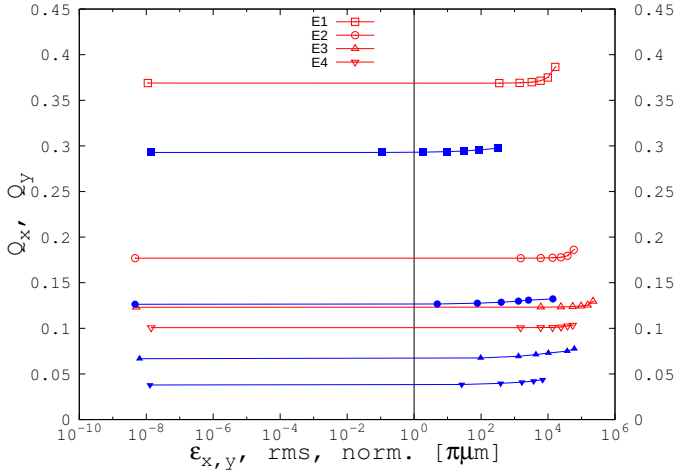

Figure 15: Amplitude detuning Q_x versus ϵ_x (empty markers, red), Q_y versus ϵ_y (filled markers, blue) at the design energies, E_1, E_2, E_3, E_4, respectively 42, 78, 114 and 150 MeV. In nominal working regime transverse emittances are in the micro-meter range (vertical bar), away from any substantial amplitude-detuning effect seen to the right. Any halo extent within two order of magnitude of $\epsilon_{x,y} = 1\,\mu$m will as well be away from substantial amplitude detuning effects.

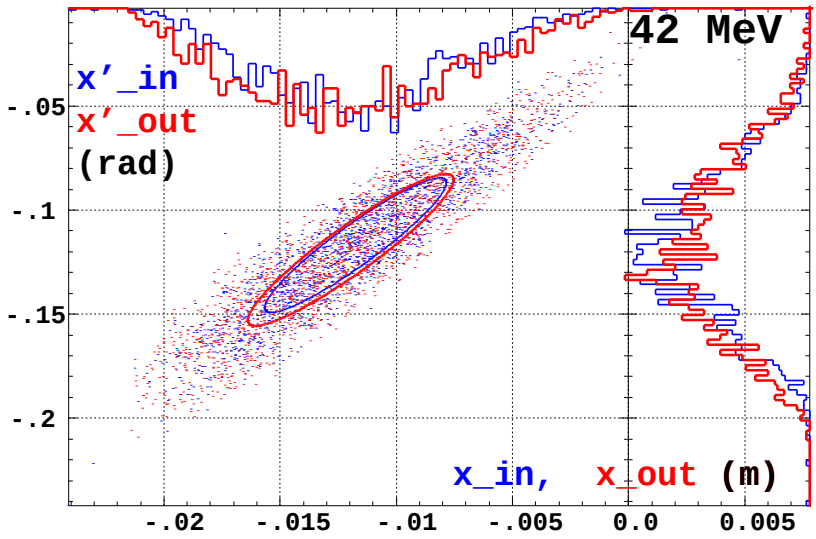

Figure 16: x,x' coordinates, initial (blue) and final (red), of the particles that make it through the 300-cell line, and *rms* matching ellipses. The geometrical emittance is $\epsilon_x/\pi = 5.7\,10^{-5}$ m, or 4.8 mm normalized.

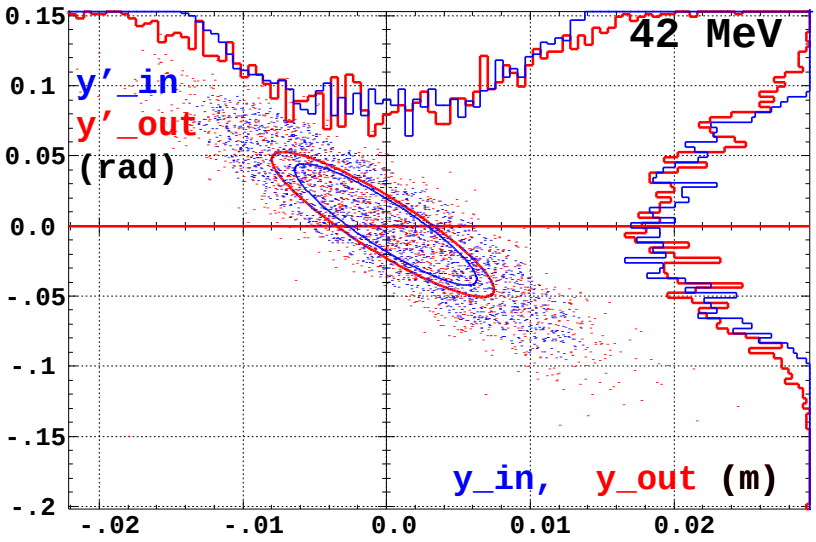

Figure 17: y, y' coordinates, initial (blue) and final (red), of the particles that make it through the 300-cell line, and *rms* matching ellipses. The geometrical emittance is $\epsilon_y/\pi = 10^{-4}$ m, or 8.4 mm normalized.

6 Comments

In conclusion to these investigations, the Halbach technology provides a CBETA cell with essentially linear properties at the four design energies, 42, 78, 144 and 150 MeV, with quasi-elliptical motion and marginal amplitude detuning up to large excursions, offering operation margins well beyond CBETA beam orbit and emittance requirements.

A global simulation of a 4-D bunch through a 300-cell line confirms these observations, with horizontal and vertical admittances of several 10^{1-2}millimeters.

The field-map based beam dynamics investigations, results and methods presented here represent on the other hand an introduction to on-going work regarding start-to-end 6-D bunch transport simulations in a complete stepwise ray-tracing based computer model of CBETA ERL.

References

[1] N. Banerjee et al., CBETA Design Report, Cornell-BNL ERL Test Accelerator, C. Mayes Ed., Cornell, June 2017.

[2] D. Trbojevic et al., CBETA - Cornell University, Brookhaven National Laboratory, Electron Energy Recovery Test Accelerator, TUOCB3, Proceedings of IPAC2017, Copenhagen, Denmark.
accelconf.web.cern.ch/AccelConf/ipac2017/papers/tuocb3.pdf.

[3] C. Johnstone et al., Fixed field circular accelerator designs, Proceedings of PAC99, New York, NY, USA.
D. Trbojevic et al., AIP Conf. Proc. 530, pages 333-338 (2000).

[4] N. Tsoupas et al., Design of a modified Halbach magnet for the CBETA project, Proceedings of AccApp'17, Quebec, Canada (2017);
Tech. NOte CBETA/020, BNL C-AD (2017).

[5] N. Tsoupas et al., The Beam Optics of the FFAG Cell of the CBETA ERL Accelerator, Proceedings of IPAC2017, Copenhagen, Denmark, accelconf.web.cern.ch/AccelConf/ipac2017/papers/mopik122.pdf.

[6] http://www.scientificcomputing.com/company-profiles/vector-fields-inc.

[7] D. Trbojevic et al., NS-FFAG for electron-ion collider in RHIC (eRHIC), Proceedings of NAPAC2013, Pasadena, CA USA.
accelconf.web.cern.ch/AccelConf/PAC2013/papers/tupba13.pdf.

[8] D. Trbojevic et al., ERL with non-scaling fixed field alternating gradient lattice for eRHIC, Proceedings of IPAC2015, Richmond, VA, USA.

[9] J. Scott Berg, Optimizing the design of linear non-scaling fixed field alternating gradient arcs for the electron rings of eRHIC, Proceedings of IPAC2016, Busan, Korea.

[10] N. Tsoupas et al., Permanent magnets for high energy nuclear physics accelerators, Proceedings of NAPAC2016, Chicago, IL, USA.

[11] Large amplitude motion in CBETA cell, F. Méot, https://www.osti.gov/scitech/biblio/1412715-large-amplitude-motion-bd_v3_x3p9_y1p5_z40-table-qf_v3_x3p9_y1p5_z40-table-cell.

[12] S.J. Brooks et al., Production of low cost, high field quality Halbach magnets, Proceedings of IPAC2017, Copenhagen, Denmark. https://www.bnl.gov/newsroom/news.php?a=212405.

[13] H. Witte, A permanent magnet quadrupole magnet for CBETA, Proceedings of IPAC2017, Copenhagen, Denmark.

[14] F.T.Cole, O CAMELOT ! A memoir of the MURA years, April 11, 1994. See sections 7.1, 15.3.
http://accelconf.web.cern.ch/AccelConf/c01/cyc2001/extra/Cole.pdf.

[15] Theme section: FFAG accelerators, BD-Newsletter 43, C.R. Prior Ed. (Aug. 2007) 14-133.

[16] This was stressed in the 1950s' MURA studies which from the beginning leaned on computer based multi-turn stepwise ray-tracing [14], as well as from the EMMA linear FFAG experiment using a similar quadrupole doublet cell [19]. and from the on-going 150 MeV scaling FFAG ring R/D in Japan [17].

[17] F. Méot, F. Lemuet, Developments in the ray-tracing code Zgoubi for 6-D multiturn tracking in FFAG rings, NIM A 547 (2005) 638-651.

[18] F. Méot, 6-D Beam Dynamics Simulations in FFAGs, pp. 42-46 in [15];
T. Planche et al., Design of a prototype gap shaping spiral dipole for a variable energy protontherapy FFAG, NIM A 604, 3 (2009) 435-442;
J. Fourrier et al., Spiral FFAG lattice design tools. Application to 6-D tracking in a proton-therapy class lattice, NIM A 589, 2 (2008) 133-142.

[19] R. Edgecock et al., EMMA - The world's first non-scaling FFAG, Proceedings of EPAC08, Genoa, Italy;
S. Machida et al., Acceleration in the linear non-scaling fixed-field alternating-gradient accelerator EMMA, Nature Physics, 10.1038/NPHYS2179 (2012);
J.S. Berg, The EMMA experiment, pp. 61-69 in [15].

[20] Y. Giboudot, F. Méot, Optical Matching of EMMA Cell Parameters Using Field Map Sets, Proceedings of PAC99, Vancouver, Canada, accelconf.web.cern.ch/AccelConf/PAC2009/papers/th5pfp040.pdf
F. Méot, Y. Giboudot, D. Kelliher, T. Yokoi, Beam Dynamics Simulations regarding the Experimental FFAG EMMA, using the on-line code, THPD023, Proceedings of IPAC10, Kyoto, Japan,
accelconf.web.cern.ch/AccelConf/IPAC10/papers/thpd023.pdf

[21] Zgoubi Users' Guide, F. Méot,
https://www.osti.gov/scitech/biblio/1062013-zgoubi-users-guide